ACS Photonics

Article

pubs.acs.org/journal/apchd5

Plasmon-Enhanced Metasurfaces for Controlling Optical Polarization

Fatema Alali,[†] Young Hwa Kim,[†] Alexander Baev,[‡] and Edward P. Furlani*[,†,‡,§]

[†]Department of Electrical Engineering, University at Buffalo SUNY, Buffalo, New York 14260, United States

[‡]Institute for Lasers, Photonics and Biophotonics, University at Buffalo SUNY, Buffalo, New York 14260, United States

[§]Department of Chemical and Biological Engineering, University at Buffalo SUNY, Buffalo, New York 14260, United States

Supporting Information

ABSTRACT: A method is proposed for controlling optical polarization using metasurfaces formed from arrays of planar chiral-patterned dielectric metamolecules with embedded achiral plasmonic nanostructures. At plasmon resonance, the subwavelength plasmonic nanoinclusions induce enhanced polarization of the surrounding dielectric, which gives rise to rotation of the polarization azimuth in the transmitted field. Full-wave electromagnetic analysis is used to investigate the optical response of various proposed media as a function of the symmetry and spacing of the metamolecules. The analysis shows that the metamolecules can be tailored to control the polarization state of light and produce frequency selective giant rotation of the polarization azimuth exceeding 10^5 deg/mm in the visible to near-infrared spectrum with relatively low loss. The proposed method opens up opportunities for the development of versatile ultrathin media that can manipulate optical polarization for novel micro-optical applications.

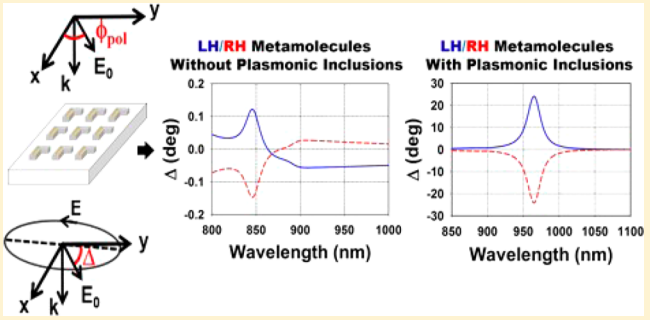

KEYWORDS: *metasurface, optical polarization rotation, plasmon-enhanced birefringence, chiral metamaterial*

Advances in nanotechnology have enabled the rapid development of artificial materials with extraordinary electromagnetic properties. The interest in such metamaterials has grown dramatically in recent years since the seminal work by Pendry.[1] Metamaterials typically consist of subwavelength constituent elements that are engineered to produce exotic electromagnetic phenomena such as negative refraction, slow light, and cloaking. As such, these materials hold promise for a transformative impact in fields that include optical imaging, sensing, communications, computing, and stealth technology, among others.

The subject of this paper is a method for realizing ultrathin metasurfaces that can be widely tailored to control the polarization state of light and produce frequency-selective giant polarization rotation with relatively low loss. Such materials open up opportunities for the miniaturization of optical components such as wave plates, polarization rotators, and circular polarizers, thereby enabling new micro-optic applications that cannot be realized using conventional optically thick components. To date, various metamaterials have been demonstrated that can be used to control optical polarization for such applications based on extraordinary linear or circular birefringence.[2−4] Examples include metallic films with subwavelength apertures,[5,6] metasurfaces with arrays of metallic nanostructures/nanoantenna,[7−13] and planar chiral metamaterials (PCMs) that consist of planar arrays of chiral metamolecules.[3,4,14−19] Many of these materials suffer from high loss, whereas the method proposed here holds potential for achieving giant birefringence with relatively low loss due to a more limited use of metallic constituents.

In this paper, we demonstrate the method via application to different metasurface designs. We study polarization rotation using numerical field analysis as illustrated in Figure 1. Here, a linearly polarized plane wave with the electric field E_0 at an angle ϕ_{pol} with respect to the x-axis is incident on a metasurface formed from chiral L-shaped dielectric metamolecules that contain an embedded achiral gold nanorod along their length. We show that this medium gives rise to an elliptically polarized transmitted field, and we compute the rotation of the polarization azimuth in the transmitted field as the angle Δ between the semimajor axis of the ellipse and the incident polarization as shown. We model three different media consisting of 2D chiral L, Z, and gammadion metamolecules, which have C_1, C_2, and C_4 (i.e., 4-fold) rotational symmetry with respect to the direction of propagation (z-axis), respectively. The first two media contain embedded Au nanorods, whereas the third utilizes a Au nanocross as the plasmonic inclusion.

Recall that an object is said to be chiral if it cannot be superimposed with its mirror image using rotations and translations alone. Helices, DNA molecules, and the crystal lattice of quartz are examples of 3D chiral structures. It should be noted that the metamolecules that we consider, absent the substrate, are not 3D chiral, as they can be rotated out of the

Received: January 18, 2014
Published: May 12, 2014

plane into their mirror image. Instead, they are chiral in a 2D or planar sense, since they cannot be superimposed with their mirror image using rotations or translations confined to the plane. However, the addition of the substrate breaks the out-of-plane rotational symmetry and renders the material 3D chiral.

The interest in PCMs stems from their unique polarizing properties. They can be engineered to produce giant polarization rotation[20−23] with asymmetric transmission of circularly and linearly polarized waves.[24−27] To date, most PCMs have been fabricated using metallic, dielectric, multilayered metallo-dielectric, and doped semiconductor array structures that are patterned into 2D chiral shapes; that is, there are no separate achiral constituents in the structures as proposed here.[14−18] However, polarization rotation has been demonstrated using planar media with achiral metallic elements alone. Examples of such media include metasurfaces with optical nanoantenna arrays[28] and PCMs with achiral metallic metamolecules.[29] The rotation in the former is due to linear birefringence and is polarization sensitive. Polarization rotation in the latter is based on the principle of extrinsic chirality, wherein the rotation is achieved at oblique incidence.[29]

As noted above, we consider three different metasurfaces with L, Z, and gammadion metamolecules, respectively. The media with L or Z metamolecules possess both linear birefringence, due to the anisotropic optical properties of the metamolecules, and circular birefringence, because these 2D chiral structures reside on a substrate, which renders the media 3D chiral. These surfaces also possess frequency-dependent linear dichroism due to the absorption properties of the embedded Au nanorods. We show that they can be tailored to exhibit giant polarization rotation due to plasmon-enhanced linear birefringence. The metasurface formed from gammadion metamolecules possesses circular birefringence[30] and frequency-dependent absorption due to the Au nanocross inclusions. We demonstrate that this medium can be tailored to produce giant polarization rotation with relatively low ellipticity based on plasmon-enhanced circular birefringence.

L METAMOLECULES

We first consider a metasurface consisting of L-shaped metamolecules as shown in Figure 1. We study its optical response using full-wave time-harmonic field analysis and solve for the E-field, which satisfies

$$\nabla \times (\mu_r^{-1} \nabla \times \mathbf{E}) - k_0^2 \left(\varepsilon_r - j\frac{\sigma}{\omega \varepsilon_0} \right) \mathbf{E} = 0 \quad (1)$$

where μ_r and ε_r are the relative permeability and permittivity of the various constituent materials, respectively. For gold nanoparticles at optical frequencies, $\mu_r = 1$, and ε_r is modeled using an analytical expression using an analytical expression that is based on the experiment-fitted critical points model of gold.[31,32] The COMSOL finite-element-based RF solver (www.comsol.com) is used for the analysis.

The computational domain for a unit cell of this media is shown in Figure 2a. This contains a single metamolecule, i.e., a dielectric L-structure with an embedded gold nanorod. We study a metamolecule with the following dimensions: height h = 200 nm, width w = 300 nm, length L = 350 nm (x-direction) and length of the short segment s = 180 nm (y-direction) (see inset in Figure 1). The dielectric is lossless and has an index of refraction of n = 1.6, which is essentially that of conventional negative photoresist SU8. The gold nanorod is 200 nm long and 80 nm

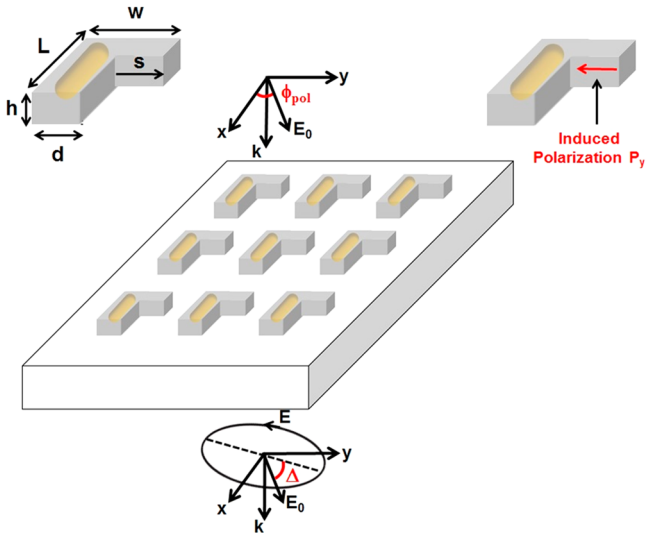

Figure 1. Linearly polarized light (E_0) incident on a 2D array of dielectric chiral L-structures with embedded gold nanorods producing elliptically polarized transmitted light with the rotation of polarization azimuth Δ.

wide and is embedded in the center of the long segment of the L-structure as shown. The L metamolecules reside on a lossless glass substrate with an index of refraction of n = 1.5. Perfectly matched layers (PMLs) are applied at the top and bottom of the computational domain to reduce backscatter from these boundaries. Computational models with the PMLs are shown in the Supporting Information. The height of the domain between the PMLs is 1500 nm along the z-axis, and the direction of propagation ($\mathbf{k}$) is downward, along the z-axis. The x- and y-dimensions of the unit cell in this case are 600 nm each, and periodic boundary conditions are applied at x and y boundaries to account for the 2D array of identical structures. Throughout this paper we assume that the incident field is a uniform downward-directed plane wave that is linearly polarized at normal incidence. The incident field is generated by a time-harmonic surface current positioned in the x−y plane directly below the upper PML.[33,34]

We first investigate the optical response with the incident E field aligned with the long segment of the L-structure, i.e., along the x-axis as shown in Figure 2a (ϕ_{pol} = 0 in Figure 1). In subsequent analysis, we will vary the direction of polarization (ϕ_{pol}) to determine its impact on the rotation spectrum. It is instructive to compare polarization rotation with and without the Au nanorod inclusion in the near-infrared (NIR) spectral range. As shown in Figure 3a, the peak rotation due to an array of lossless L-structures occurs at 846 nm and is approximately 0.12 degree for a metamolecule thickness of h = 200 nm. Note that the rotation for the right-handed (Δ_{RH}) vs left-handed (Δ_{LH}) structures has an opposite sign as expected. The same dielectric structure with an embedded Au nanorod produces a peak rotation Δ = 24.1 degrees at 965 nm, as shown in Figure 3b. This peak occurs near the absorption resonance of the nanorod, which is 974 nm. The rotation Δ depends on both the magnitude and phase of the field components E_x and E_y in the transmitted field. The induced polarization P_y that produces a transmitted E_y is mainly dependent on the near-field (NF) around the plasmonic inclusion. However, E_x is more affected (attenuated) by absorption. Since the rotation is a function of both of these components, it has a complex dependency on NF enhancement

dx.doi.org/10.1021/ph5000192 | ACS Photonics 2014, 1, 507−515

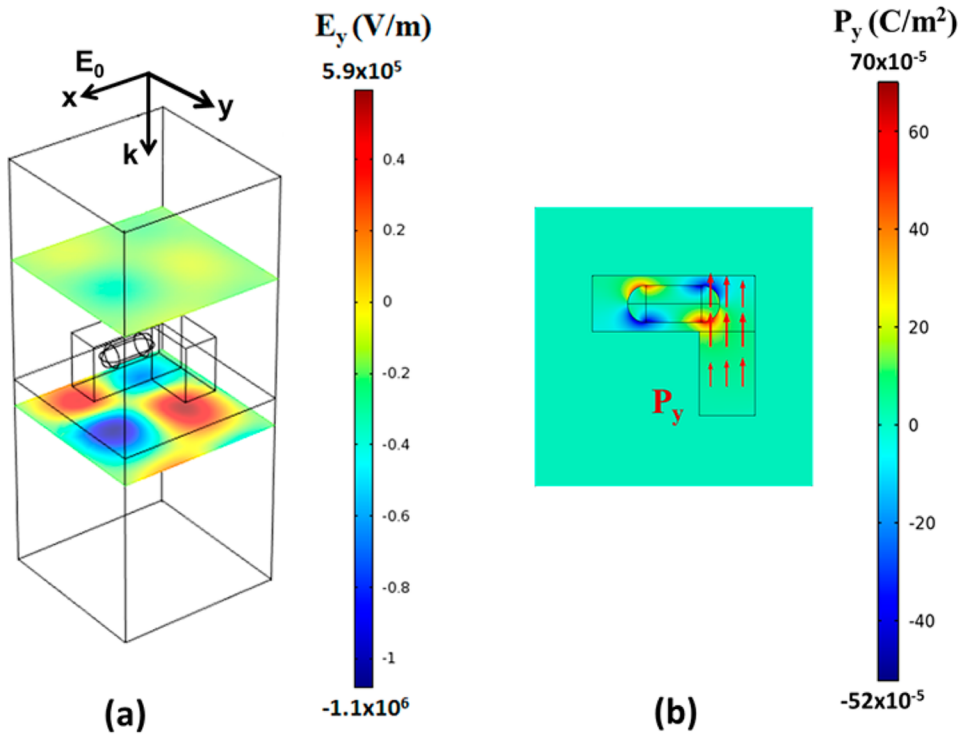

Figure 2. L metamolecule: (a) computational model for a unit cell and field analysis showing E_y in the transmitted field with the incident polarization along the x-axis ($\phi_{pol} = 0°$); (b) plasmon-enhanced polarization P_y in the short segment of the L, orthogonal to the incident polarization.

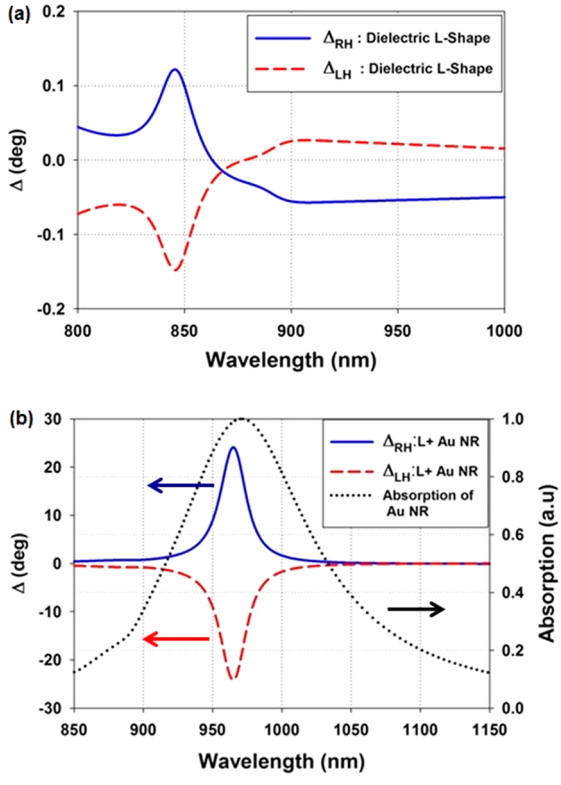

Figure 3. Polarization rotation spectra: (a) for an array of right-handed (solid blue line) and left-handed (dashed red line) lossless dielectric L-structures on a substrate and (b) for an array of right -handed (solid blue line) and left-handed (dashed red line) L-structures with an embedded Au nanorod. The normalized absorption spectrum is also plotted (dotted black line).

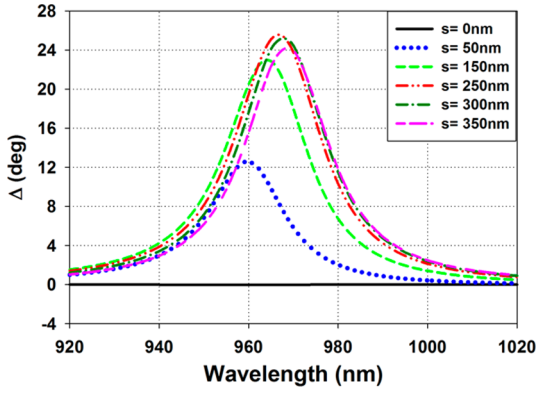

Figure 4. L metamolecule: polarization rotation vs s (length of short L-segment).

and absorption. Moreover, these effects typically have different spectral profiles and resonant wavelengths, especially for larger particles, e.g., with dimensions on the same order as the wavelength. These differences are due to phenomena such as depolarization of the radiation across the particle and radiative damping.[8,35−37] To this point, the embedded nanorods that we study are 200 nm long, which is an appreciable fraction of the incident wavelength (e.g., 800−1100 nm). Therefore, it is not surprising that the rotation and absorption peak are offset from each other in a spectral sense as observed.

Note that the peak rotation we obtain represents a 2000-fold increase in rotation Δ over the same structure without the Au nanorod and corresponds to a giant specific polarization rotation of 1.2×10^5 deg/mm. As a point of comparison, the specific rotation of quartz is 13.3 deg/mm at $\lambda = 730.7$ nm. It should be noted that throughout this paper the specific rotation is calculated based on the thickness of the metamolecules alone,

dx.doi.org/10.1021/ph5000192 | ACS Photonics 2014, 1, 507−515

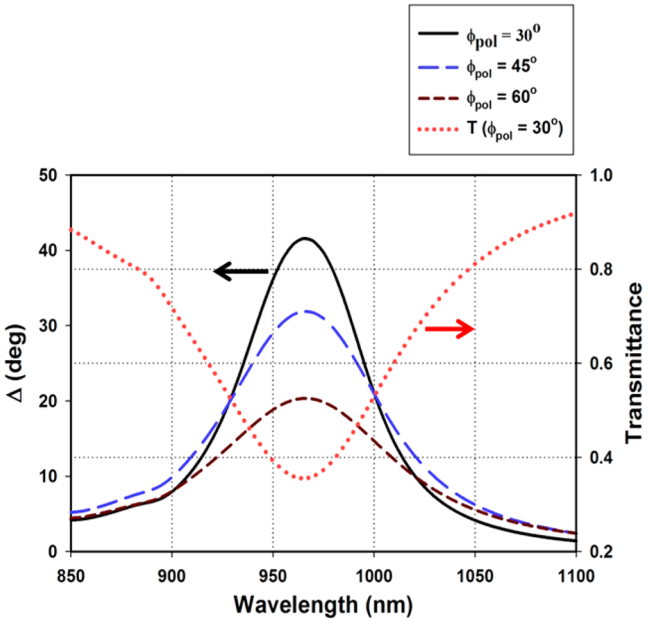

Figure 5. L metamolecule: polarization rotation Δ vs polarization (ϕ_{pol}) and transmittance for ϕ_{pol} = 30°.

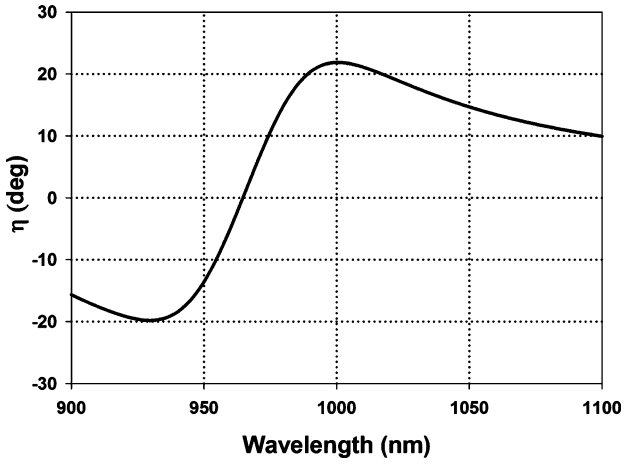

Figure 6. L metamolecule: ellipticity for ϕ_{pol} = 30°.

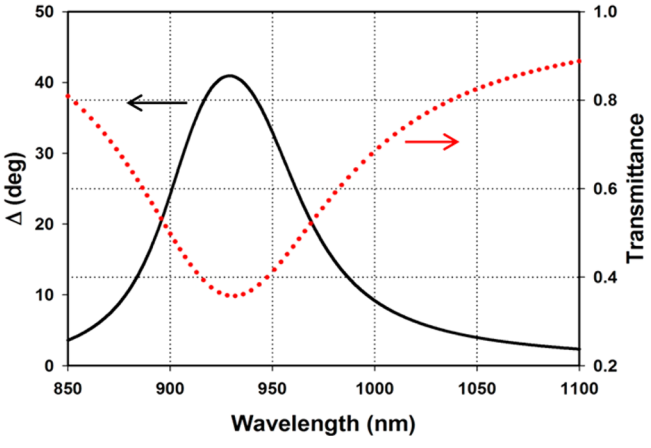

Figure 7. L metamolecule: polarization rotation and transmittance without a substrate (ϕ_{pol} = 30°).

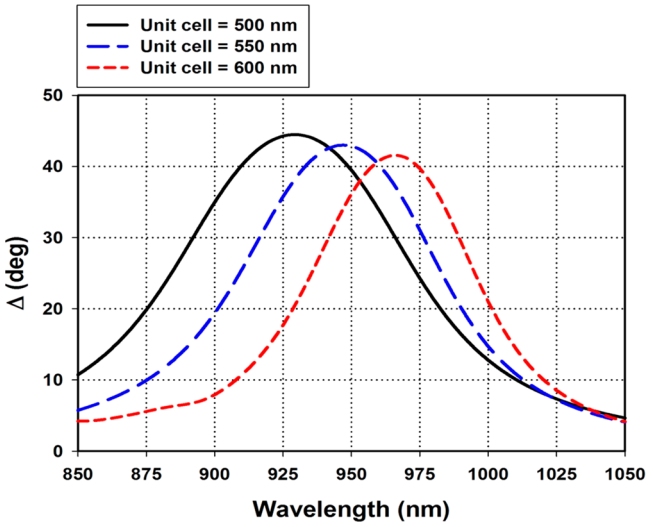

Figure 8. L metamolecule: rotation vs size of the unit cell (ϕ_{pol} = 30°).

i.e., neglecting the thickness of the substrate. We show that the substrate has little impact on the magnitude of the rotation in a subsequent analysis. Also, while it is instructive to compare the rotational performance of the metasurface to a bulk material, it should be kept in mind that if a scaled-up "bulk" metametarial is formed from layers of such metasurfaces, the near-field coupling between neighboring layers might degrade the optical performance.

The giant rotation of the polarization azimuth with ϕ_{pol} = 0 is due to plasmon-enhanced polarization of the chiral-patterned dielectric, predominantly polarization P_y in the short segment (s) of the L-structure as shown in the right-side inset of Figure 1 and in Figure 2b. The plasmon-enhanced magnitude of P_y is 4.5 × 10^{-5} C/m^2 at the center of the segment. This is 2 orders of magnitude greater than the corresponding value of 4.1 × 10^{-7} C/m^2 that is obtained without the nanorod. Since P_y is orthogonal to the incident field, $E_0 = E_x$, it produces a corresponding scattered field component E_y (shown in Figure 2a), which gives rise to an elliptically polarized transmitted field with a polarization azimuth that is rotated with respect to the incident field as illustrated in Figure 1.

An additional study of the effects of the induced P_y is shown in Figure 4. Here, we consider the L metamolecule of Figure 1 and investigate rotation as a function of the length s of the short segment (see left-side inset in Figure 1). For s = 0 nm, we have a single Au nanorod embedded in an achiral rectangular I-structure. Although plasmon resonance of the nanorod is excited, this shape cannot support a net P_y when the incident polarization is along the nanorod (for ϕ_{pol} = 0). Consequently, there is no rotation, as shown in Figure 4. However, as s increases, Δ increases and there is a slight red-shift in the rotation spectrum. The increase in rotation is due to an increase in the magnitude of the induced P_y in the short segment of the L. The red-shift is due to an increase in the ambient dielectric constant around the nanorod that occurs as the short dielectric segment increases and replaces free space. As shown in the figure, the maximum peak rotation in the spectral plots occurs when s = 250 nm. After that, the peak rotation very gradually decreases but continues to red-shift.

Next, we investigate rotation as a function of the incident polarization. We compute the rotation spectra with the incident polarization set at three different angles, ϕ_{pol} = 30°, 45°, 60°, as

dx.doi.org/10.1021/ph5000192 | ACS Photonics 2014, 1, 507−515

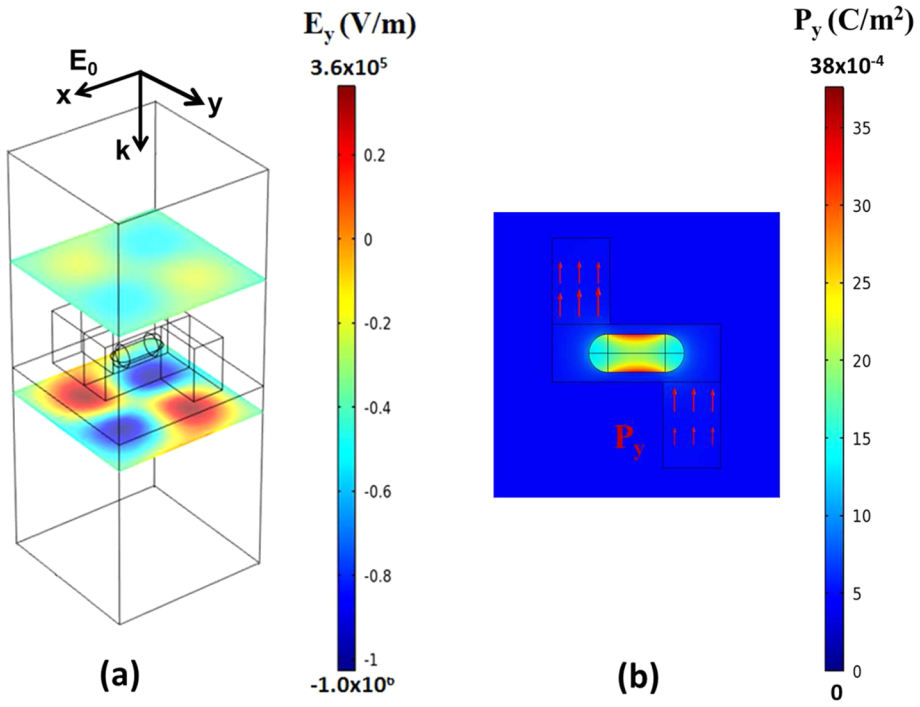

Figure 9. Z metamolecule: (a) computational model and field analysis showing E_y in the transmitted field for a unit cell with the incident polarization along the x-axis ($\phi_{pol} = 0°$); (b) plasmon-enhanced polarization P_y, orthogonal to the incident polarization.

measured with respect to the x-axis (see Figure 1). Figure 5 clearly shows that the rotation is polarization sensitive, which is due to the linear birefringence of the media. The peak rotation for each value of ϕ_{pol} occurs near the plasmon resonance of the nanorod, and an overall maximum rotation $\Delta = 41.55°$ occurs when $\phi_{pol} = 30°$. This corresponds to a giant specific rotation of 2.08×10^5 deg/mm. The transmittance is 35.5% at the peak rotation. The ellipticity η of the transmitted field for $\phi_{pol} = 30°$ is plotted as a function of wavelength in Figure 6.

It is instructive to examine the effect of the chiral-patterned dielectric layer on the optical response of the metasurface. To this end, we eliminate this layer and analyze a 2D array of bare nanorods on a substrate using the same dimensions as above. The nanorods give rise to linear birefringence as before, but we find that the peak rotation at $\phi_{pol} = 30°$ is only 12°, which is less than 30% of the value obtained with the patterned dielectric. Moreover, there is no rotation when the field is aligned with the nanorods ($\phi_{pol} = 0°$), which is in sharp contrast to the giant rotation, $\Delta = 24.1°$, obtained when the nanorods are encapsulated. We performed a similar analysis with the nanorods embedded in a uniform (unpatterned) dielectric layer and found that the peak rotation was also less that obtained with the patterning. The patterned dielectric layer produced a larger rotation over a broader range of polarizations than either bare nanorods or the nanorods embedded within a uniform dielectric.

We also determine the impact of the substrate on Δ. To do so, we set the permittivity of the substrate to that of free space and compute the rotation and transmittance spectra with $\phi_{pol} = 30°$. These profiles are plotted in Figure 7 and are substantially the same as those obtained with the substrate present (Figure 5), except slightly blue-shifted due to a decrease in the ambient dielectric constant. The substrate has a negligible effect on rotation because the latter is principally due to the linear birefringence of metamolecules. Thus, it is appropriate to compute the specific rotation of the polarization azimuth for this medium using the thickness of the metamolecules alone, i.e., ignoring the thickness of the substrate.

The dependence of rotation on the lattice spacing between the metamolecules is also of interest. We investigate this by computing the rotation spectra with the polarization at $\phi_{pol} = 30°$ for three different square unit cells, i.e., 500, 550, and 600 nm on a side, respectively. These data, which are plotted in Figure 8, show that as the lattice spacing decreases, the peak rotation increases and the spectrum blue-shifts to shorter wavelengths. This is due to the near-field plasmonic coupling between the longitudinal resonances of nanorods, analogous to exciton coupling in H-aggregates of organic chromophores.[38] To verify this, we repeated the analysis with all of the dielectric material in the computational domain replaced by free space, i.e., leaving only a 2D array of nanorods. We observed a similar blue-shift in the absorption spectra as the lattice spacing decreased.

Z METAMOLECULES

We now consider the Z-shaped metamolecules. These are formed by adding an additional short dielectric segment symmetrically to the L-structure, which results in a C_2 rotational symmetry. The dimensions and material properties are the same as for the L-structure, and we repeat the same analysis as above. A computational model is shown in Figure 9. Here, the unit cell is square, 600 nm on a side, and the incident polarization is along the x-axis. Figure 9a shows surface plots of E_y above and below the metamolecule, and Figure 9b shows the induced polarization P_y that gives rise to E_y.

As a first step, we compare the polarization rotation for L- and Z-shaped metamolecules when the incident field is aligned with the nanorods ($\phi_{pol} = 0°$). It is instructive to also consider an achiral C-shaped metamolecule to emphasize the structural dependence of the plasmon-enhanced polarization and its effect on rotation. The rotation spectra for the three structures are shown in Figure 10. Note that the Z metamolecule produces the

dx.doi.org/10.1021/ph5000192 | ACS Photonics 2014, 1, 507−515

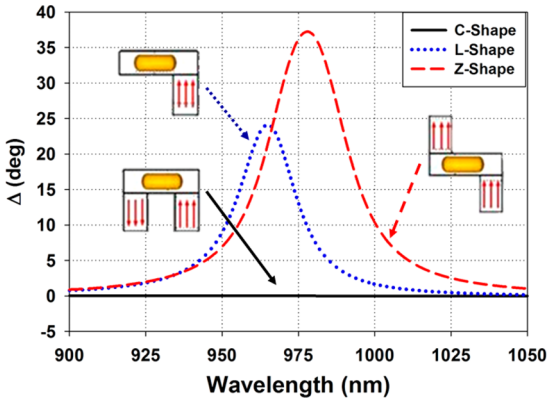

Figure 10. Polarization rotation for L-, Z-, and C-shaped metamolecules with ϕ_{pol} = 0°; red arrows indicate direction of induced dielectric polarization.

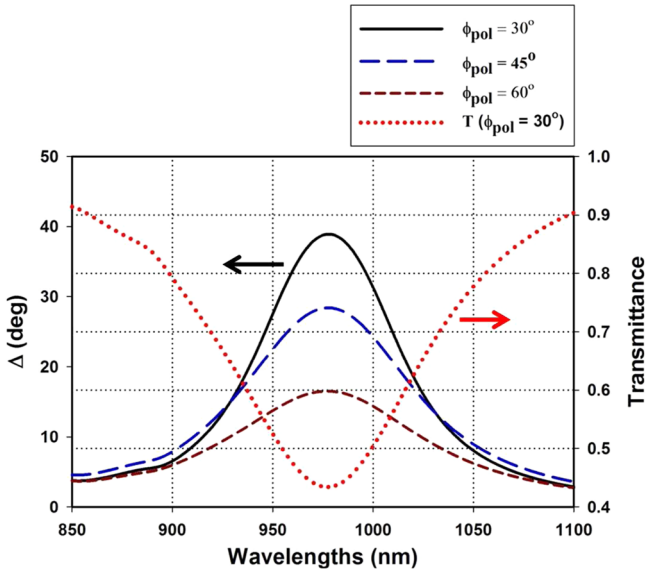

Figure 11. Z metamolecule: rotation spectra vs polarization (ϕ_{pol}) and transmittance at ϕ_{pol} = 30°.

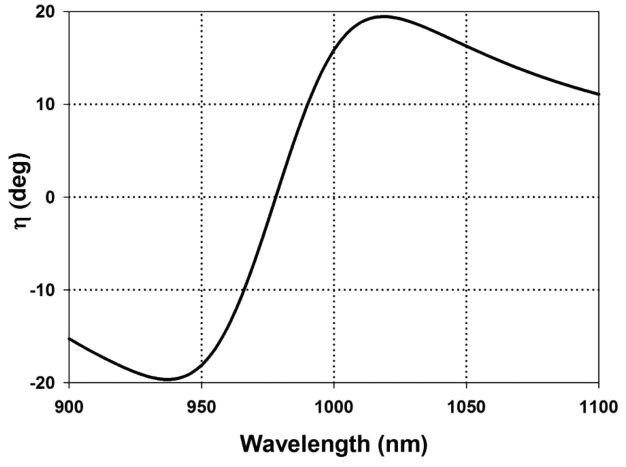

Figure 12. Z metamolecule: ellipticity for ϕ_{pol} = 30°.

largest rotation, while the C metamolecule produces no rotation. The Z metamolecule produces more rotation than the L metamolecule because P_y components are induced in each of its short segments, and these are in phase as indicated by the red

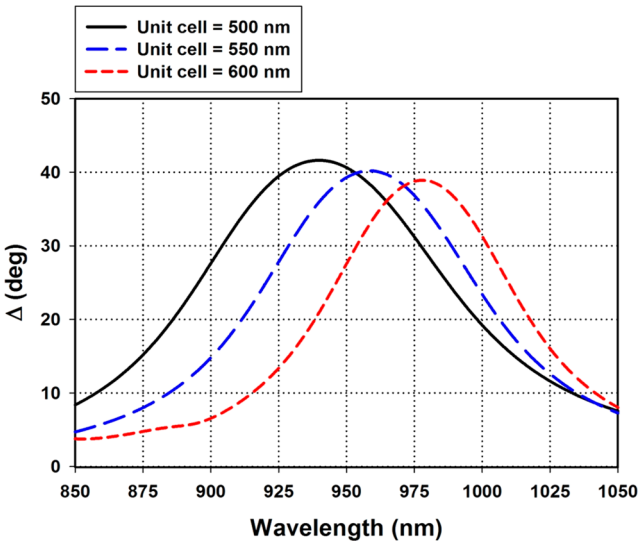

Figure 13. Z metamolecule: rotation vs size of the unit cell for ϕ_{pol} = 30°.

polarization arrows. The L metamolecule has only one short segment and therefore less net induced polarization. As for the C metamolecule, its short segments are polarized, but the polarizations are 180° out of phase and their effects cancel.

Next we compute the rotation spectra for the Z metamolecules with the incident polarization at three different angles, ϕ_{pol} = 30°, 45°, and 60°, and the transmittance spectrum for ϕ_{pol} = 30°. As shown in Figure 11, these profiles are similar to those obtained for the L metamolecules; however the peak rotations are slightly lower, the transmittance is slightly higher, and the rotation spectra are red-shifted due to an increase in ambient dielectric material in proximity to the nanorod (i.e., the additional dielectric segment that forms the Z). The maximum rotation is Δ = 38.84° at λ = 980 nm when ϕ_{pol} = 30°, which corresponds to a giant specific rotation of 1.942 × 10^5 deg/mm. The transmittance is 43.52% at this peak. We also found that the same level of rotation is obtained without the substrate, similar to that of the L metamolecule (see Figure 7). The ellipticity of the transmitted field for ϕ_{pol} = 30° is shown in Figure 12 and is similar to that of the L metamolecule as well (see Figure 6).

Lastly, we compute the rotation spectra for ϕ_{pol} = 30° as a function of the lattice spacing for square unit cells, 500, 550, and 600 nm on a side. These are plotted in Figure 13 and exhibit a similar behavior to those obtained for the L metamolecules; that is, as the cell size decreases, the spectra blue shift and the peak rotation increases slightly due to an increase in plasmonic coupling between the nanorods.

GAMMADION METAMOLECULES

The last metasurface we consider consists of an array of gammadion metamolecules with an embedded achiral Au cross. The metamolecules have C_4 rotational symmetry, which gives rise to a rotation Δ that is independent of the incident polarization. The computational model for a unit cell is shown in Figure 14a. The gammadion is 200 nm in height and has a square cross-section that spans 350 nm on each side. The width of the constituent segments is 100 nm. The embedded Au cross is 150 nm high, 80 nm wide, 300 nm end-to-end, and centered in the dielectric as shown in Figure 14b.

The gammadion array has a lattice spacing of 450 nm. A representative rotation spectrum and corresponding transmittance are shown in Figure 15. Note that a peak rotation of

dx.doi.org/10.1021/ph5000192 | ACS Photonics 2014, 1, 507−515

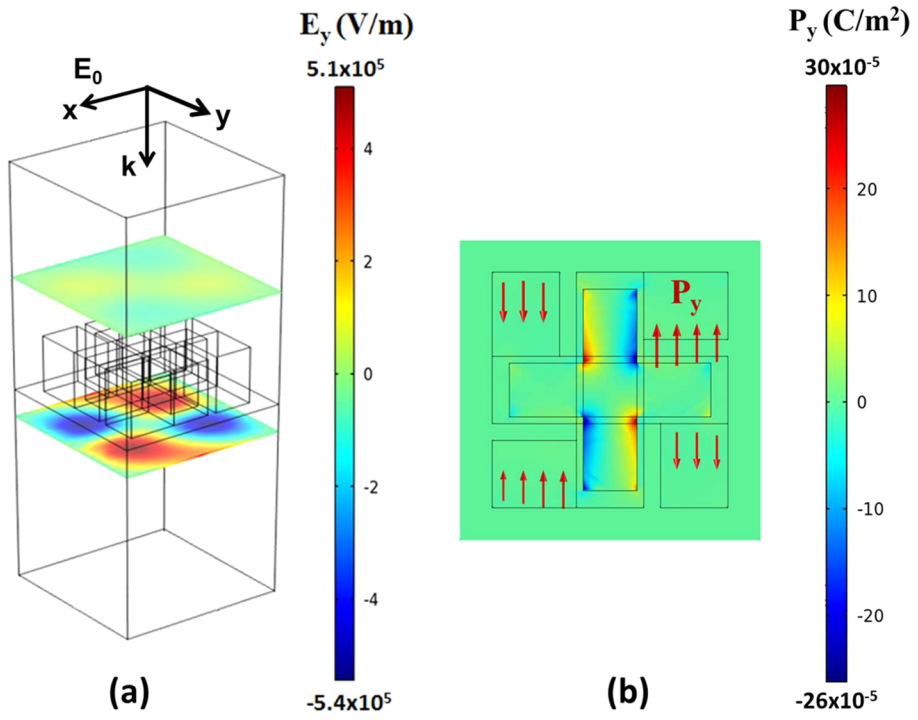

Figure 14. Gammadion metamolecule: (a) computational model and field analysis showing E_y in the transmitted field for a unit cell with the incident polarization along the x-axis ($\phi_{pol} = 0°$); (b) plasmon-enhanced polarization P_y, orthogonal to the incident polarization.

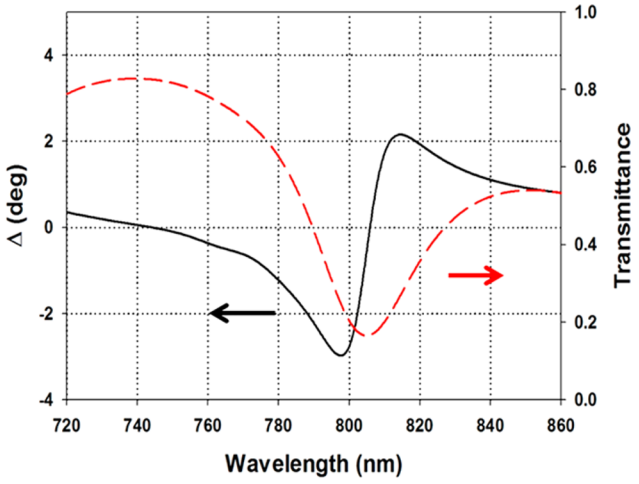

Figure 15. Gammadion metamolecule: rotation spectra and transmittance.

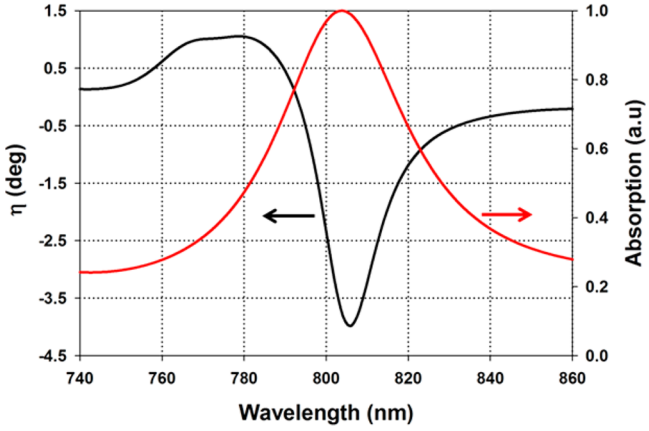

Figure 16. Gammadion metamolecule: ellipticity and absorption spectra.

3° is obtained at $\lambda = 798$ nm with a corresponding transmittance of approximately 24%. This corresponds to a giant specific rotation of 1.5×10^4 deg/mm near the absorption resonance of the Au cross, which occurs at $\lambda = 804$ nm. Note that the peak rotation is an order of magnitude lower than that obtained with the L or Z metamolecules. A similar analysis for an all dielectric gammadion, i.e., without the gold cross, resulted in a peak rotation of less than 0.1°. Thus, plasmon enhancement produces more than a 30-fold increase in the rotation. It is important to note that the giant specific rotation obtained here is greater than that reported for purely metallic (Au) gammadion metamolecules, and the transmittance is higher because of the reduced metallic content.[22] Specifically, a fabricated metasurface consisting of a 2D array of 95 nm high Au gammadions with a lattice spacing of 500 nm exhibited a peak rotation of polarization of approximately 1.5° at $\lambda = 640$ nm and a transmission of less than 10% at this wavelength (see Figure 2 of ref 22). By way of comparison, the proposed metamolecules have a similar lattice spacing and essentially twice the height as their Au counterparts, and they produce more than twice the rotation and transmission.

The embedded Au cross gives rise to circular dichroism (CD), i.e., a differential absorption of right and left circularly polarized (RCP and LCP) light. The linearly polarized incident field can be decomposed into RCP and LCP components, which acquire different amplitudes as they pass through the metasurface. The superposition of these components in the transmitted field yields elliptically polarized light, with a polarization that is rotated with respect to the incident field. The change in the sign of the rotation near the absorption resonance (in this case negative to positive) as shown in Figures 15 and 17 is a characteristic of chiral behavior and depends on the handedness of the metamolecule.

dx.doi.org/10.1021/ph5000192 | ACS Photonics 2014, 1, 507−515

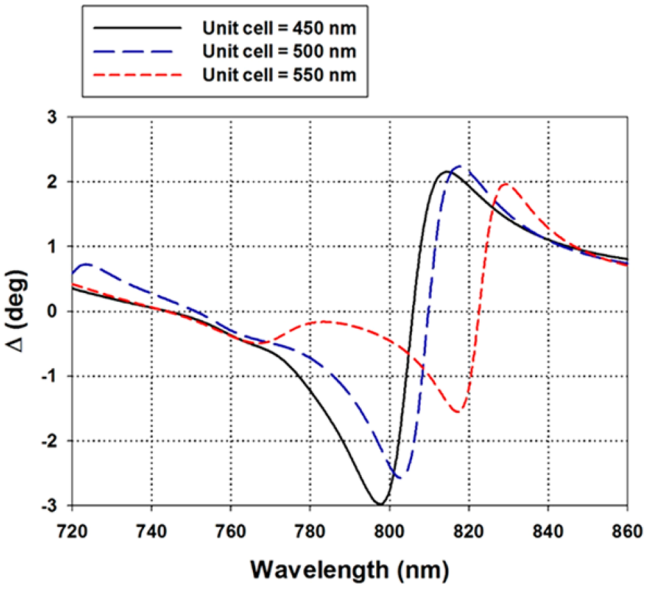

Figure 17. Gammadion metamolecule: polarization rotation vs the size of the unit cell.

The ellipticity η and normalized absorption spectra for the metamolecule are plotted in Figure 16. The peak ellipticity occurs near the absorption resonance and is relatively low, which implies that the transmitted polarization is nearly linear.

Finally, we investigate the rotation spectrum as a function of the metamolecule lattice spacing for square unit cells that are 450, 500, and 550 nm on a side, respectively. We find that as the lattice spacing decreases, the rotation spectra have the same general form, but the peak rotation increases and the rotation spectrum blue-shifts as shown in Figure 17. These effects are due to enhanced plasmonic coupling between neighboring metamolecules that occurs when the intermolecule spacing decreases.

CONCLUSIONS

We have introduced a method for controlling optical polarization at normal incidence using ultrathin metasurfaces formed from arrays of subwavelength chiral-patterned dielectric metamolecules that contain achiral plasmonic inclusions. Giant polarization rotation can be obtained near the absorption resonance of the inclusions, which is due to enhanced polarization of the encapsulating dielectric. The size, shape, and spacing of the metamolecules can be widely tailored to produce frequency-selective rotation in the visible to NIR spectrum with relatively low loss. We have found that polarization-sensitive giant specific rotation in excess of 10^5 deg/mm can be realized at normal incidence with linear birefringent media that exhibit C_1 and C_2 rotational symmetry. A corresponding polarization-independent rotation exceeding 10^4 deg/mm can be obtained with relatively low ellipticity using C_4 symmetric metamolecules. This level of rotation is greater than that reported for media containing purely metallic chiral metamolecules,[22] and the transmittance is higher because of the relatively lower metallic content. We have also shown that a chiral-patterned dielectric layer provides higher polarization rotation over a broader range of incident polarization angles than a corresponding media with an unpatterned layer. Also, it is worth noting that we initially considered the partial embedding of plasmonic elements in a patterned dielectric, but found that this resulted in much lower polarization rotation as compared to fully embedded nanoinclusions. Moreover, we found that the embedded inclusions need to be carefully sized and positioned within the dielectric to optimize the polarization rotation. The proposed metasurfaces lend themselves to intuitive designs, as their optical response is based primarily on the plasmonic behavior of well-studied achiral nanostructures, and they can be fabricated using a variety of top-down techniques such as stencil lithography[39] The approach presented here should stimulate research at the intersection of chiral photonics and plasmonics and lead to a new class of ultrathin materials for manipulating the polarization of light.

ASSOCIATED CONTENT

Supporting Information

Further details of the computational models used for predicting the optical response of the metasurfaces are provided. This material is available free of charge via the Internet at http://pubs.acs.org.

AUTHOR INFORMATION

Corresponding Author

*E-mail: efurlani@buffalo.edu. Phone: (716) 645-1194. Fax: (716) 645-3822.

Notes

The authors declare no competing financial interest.

REFERENCES

(1) Pendry, J. B. A Chiral Route to Negative Refraction. *Science* **2004**, *306*, 1353−1355.
(2) Kildishev, A. V.; Boltasseva, A.; Shalaev, V. M. Planar Photonics with Metasurfaces. *Science* **2013**, *339*, 6125.
(3) Valev, V. K.; Baumberg, J. J.; Sibilia, C.; Verbiest, T. Chirality and Chiroptical Effects in Plasmonic Nanostructures: Fundamentals, Recent Progress, and Outlook. *Adv. Mater.* **2013**, *25*, 2517−2534.
(4) Wang, B.; Zhou, J.; Koschny, T.; Kafesaki, M.; Soukoulis, C. M. Chiral Metamaterials: Simulations and Experiments. *J. Opt. A: Pure Appl. Opt.* **2009**, *11*, 114003.
(5) Wang, L.; Hu, H. F.; Liu, K.; Jiang, S. H.; Zeng, W.; Gan, Q. Q. Polarization Management of Terahertz Extraordinary Optical Transmission through Ultracompact L-Shaped Subwavelength Patterns on Metal Films. *Plasmonics* **2013**, *8*, 733−740.
(6) Gorodetski, Y.; Shitrit, N.; Bretner, I.; Kleiner, V.; Hasman, E. Observation of Optical Spin Symmetry Breaking in Nanoapertures. *Nano Lett.* **2009**, *9*, 3016−3019.
(7) Zhao, Y.; Alù, A. Manipulating Light Polarization with Ultrathin Plasmonic Metasurfaces. *Phys. Rev. B* **2011**, *84*, 205428.
(8) Yu, N.; Genevet, P.; Aieta, F.; Kats, M.; Blanchard, R.; Aoust, G.; Tetienne, J.; Gaburro, Z.; Capasso, F. Flat Optics: Controlling Wavefronts with Optical Antenna Metasurfaces. *IEEE J. Sel. Top. Quantum Electron.* **2013**, *19*, 4700423.
(9) Yu, N.; Aieta, F.; Genevet, P.; Kats, M. A.; Gaburro, Z.; Capasso, F. A Broadband, Background-Free Quarter-Wave Plate Based on Plasmonic Metasurfaces. *Nano Lett.* **2012**, *12*, 6328−6333.
(10) Zhao, Y.; Alù, A. Tailoring the Dispersion of Plasmonic Nanorods to Realize Broadband Optical Meta-Waveplates. *Nano Lett.* **2013**, *13*, 1086−1091.
(11) Biagioni, P.; Savoini, M.; Huang, J. S.; Duò, L.; Finazzi, M.; Hecht, B. Near-Field Polarization Shaping by a Near-Resonant Plasmonic Cross Antenna. *Phys. Rev. B* **2009**, *80*, 153409.
(12) Pors, A.; Nielsen, M. G.; Valle, G. D.; Willatzen, M.; Albrektsen, O.; Bozhevolnyi, S. I. Plasmonic Metamaterial Wave Retarders in Reflection by Orthogonally Oriented Detuned Electrical Dipoles. *Opt. Lett.* **2011**, *36*, 1626−1628.
(13) Ellenbogen, T.; Seo, K.; Crozier, K. B. Chromatic Plasmonic Polarizers for Active Visible Color Filtering and Polarimetry. *Nano Lett.* **2012**, *12*, 1026−1031.

(14) Plum, E.; Zhou, J.; Dong, J.; Fedotov, V. A.; Koschny, T.; Soukoulis, C. M.; Zheludev, N. I. Metamaterial with Negative Index Due to Chirality. *Phys. Rev. B* **2009**, *79*, 035407.
(15) Decker, M.; Ruther, M.; Kriegler, C. E.; Zhou, J.; Soukoulis, C. M.; Linden, S.; Wegener, M. Strong Optical Activity from Twisted-Cross Photonic Metamaterials. *Opt. Lett.* **2009**, *34*, 2501−2503.
(16) Bai, B.; Svirko, Y.; Turunen, J.; Vallius, T. Optical Activity in Planar Chiral Metamaterials: Theoretical Study. *Phys. Rev. A* **2007**, *76*, 023811.
(17) Schaferling, M.; Dregely, D.; Hentschel, M.; Giessen, H. Tailoring Enhanced Optical Chirality: Design Principles for Chiral Plasmonic Nanostructures. *Phys. Rev. X* **2012**, *2*, 031010.
(18) Decker, M.; Zhao, R.; Soukoulis, C. M.; Linden, S.; Wegener, M. Twisted Split-Ring-Resonator Photonic Metamaterial with Huge Optical Activity. *Opt. Lett.* **2010**, *35*, 1593−1595.
(19) Vallius, T.; Jefimovs, K.; Turunen, J.; Vahimaa, P.; Svirko, Y. Optical Activity in Subwavelength-Period Arrays of Chiral Metallic Particles. *Appl. Phys. Lett.* **2003**, *83*, 234−236.
(20) Furlani, E. P.; Jee, H. S.; Oh, H. S.; Baev, A.; Prasad, P. N. Laser Writing of Multiscale Chiral Polymer Metamaterials. *Adv. OptoElectron.* **2012**, 861569.
(21) Papakostas, A.; Potts, A.; Bagnall, D. M.; Prosvirnin, S. L.; Coles, H. J.; Zheludev, N. I. Optical Manifestations of Planar Chirality. *Phys. Rev. Lett.* **2003**, *90*, 107404.
(22) Kuwata-Gonokami, M.; Saito, N.; Ino, Y.; Kauranen, M.; Jefimovs, K.; Vallius, T.; Turunen, J.; Svirko, Y. Giant Optical Activity in Quasi-Two-Dimensional Planar Nanostructures. *Phys. Rev. Lett.* **2005**, *95*, 227401.
(23) Jefimovs, K.; Saito, N.; Ino, Y.; Vallius, T.; Vahimaa, P.; Turunen, J.; Shimano, R.; Kauranen, M.; Svirko, Y.; Kuwata-Gonokami, M. Optical Activity in Chiral Gold Nanogratings. *Microelectron. Eng.* **2005**, *78*−*79*, 448−451.
(24) Zhang, W.; Potts, A.; Bagnall, D. M. Giant Optical Activity in Dielectric Planar Metamaterials with Two-Dimensional Chirality. *J. Opt. A: Pure Appl. Opt.* **2006**, *8*, 878−890.
(25) Fedotov, V. A.; Mladyonov, P. L.; Prosvirnin, S. L.; Rogacheva, A. V.; Chen, Y.; Zheludev, N. I. Asymmetric Propagation of Electromagnetic Waves through a Planar Chiral Structure. *Phys. Rev. Lett.* **2006**, *97*, 167401.
(26) Schwanecke, A. S.; Fedotov, V. A.; Khardikov, V. V.; Prosvirnin, S. L.; Chen, Y.; Zheludev, N. I. Nanostructured Metal Film with Asymmetric Optical Transmission. *Nano Lett.* **2008**, *8*, 2940−2943.
(27) Plum, E.; Fedotov, V. A.; Zheludev, N. I. Planar Metamaterial with Transmission and Reflection that Depend on the Direction of Incidence. *Appl. Phys. Lett.* **2009**, *94*, 131901.
(28) Plum, E.; Fedotov, V. A.; Zheludev, N. I. Asymmetric Transmission: A Generic Property of Two-Dimensional Periodic Patterns. *J. Opt.* **2011**, *13*, 024006.
(29) Kats, M. A.; Genevet, P.; Aoust, G.; Yu, N. F.; Blanchard, R.; Aieta, F.; Gaburro, Z.; Capasso, F. Giant Birefringence in Optical Antenna Arrays with Widely Tailorable Optical Anisotropy. *Proc. Natl. Acad. Sci. U.S.A.* **2012**, *109*, 12364−12368.
(30) Plum, E.; Liu, X. X.; Fedotov, V. A.; Chen, Y.; Tsai, D. P.; Zheludev, N. I. Metamaterials: Optical Activity without Chirality. *Phys. Rev. Lett.* **2009**, *102*, 113902.
(31) Etchegoin, P. G.; Le Ru, E. C.; Meyer, M. An Analytic Model for the Optical Properties of Gold. *J. Chem. Phys.* **2006**, *125*, 164705.
(32) Etchegoin, P. G.; Le Ru, E. C.; Meyer, M. Erratum: "An Analytic Model for the Optical Properties of Gold" [*J. Chem. Phys.* **2006**, *125*, 164705]. *J. Chem. Phys.* **2007**, *127*, 189901.
(33) Furlani, E. P.; Baev, A. Optical Nanotrapping Using Cloaking Metamaterial. *Phys. Rev. E* **2009**, *79*, 026607.
(34) Furlani, E. P.; Baev, A. Free-space Excitation of Resonant Cavities Formed from Cloaking Metamaterial. *J. Mod. Opt.* **2009**, *56*, 523−529.
(35) Ross, B. M.; Tasoglu, S.; Lee, L. P. Plasmon Resonance Differences between the Near- and Far-Field and Implications for Molecular Detection. *Proc. SPIE 7394, Plasmonics: Metallic Nanostructures and Their Optical Properties VII*; 2009; pp 739422−739422.
(36) Kelly, K. L.; Coronado, E.; Zhao, L. L.; Schatz, G. C. The Optical Properties of Metal Nanoparticles: The Influence of Size, Shape, and Dielectric Environment. *J. Phys. Chem. B* **2003**, *107*, 668−677.
(37) Kats, M. A.; Yu, N.; Genevet, P.; Gaburro, Z.; Capasso, F. Effect of Radiation Damping on the Spectral Response of Plasmonic Components. *Opt. Express* **2011**, *19*, 21748−21753.
(38) Jain, P. K.; Eustis, S.; El-Sayed, M. A. Plasmon Coupling in Nanorod Assemblies: Optical Absorption, Discrete Dipole Approximation Simulation, and Exciton-Coupling Model. *J. Phys. Chem. B* **2006**, *110*, 18243−18253.
(39) Vazquez-Mena, O.; Sannomiya, T.; Tosun, M.; Villanueva, L. G.; Savu, V.; Voros, J.; Brugger, J. High-Resolution Resistless Nanopatterning on Polymer and Flexible Substrates for Plasmonic Biosensing Using Stencil Masks. *ACS Nano* **2012**, *6*, 5474−5481.